J. Fluid Mech. (1977), *vol.* 79, *part* 1, *pp.* 127–156
Printed in Great Britain

Rotating elliptic cylinders in a viscous fluid at rest or in a parallel stream

By HANS J. LUGT AND SAMUEL OHRING
David W. Taylor Naval Ship Research and Development Center, Bethesda, Maryland 20084

(Received 11 June 1976)

Numerical solutions are presented for laminar incompressible fluid flow past a rotating thin elliptic cylinder either in a medium at rest at infinity or in a parallel stream. The transient period from the abrupt start of the body to some later time (at which the flow may be steady or periodic) is studied by means of streamlines and equi-vorticity lines and by means of drag, lift and moment coefficients. For purely rotating cylinders oscillatory behaviour from a certain Reynolds number on is observed and explained. Rotating bodies in a parallel stream are studied for two cases: (i) when the vortex developing at the retreating edge of the thin ellipse is in front of the edge and (ii) when it is behind the edge.

1. Brief review

Laminar flow of an incompressible fluid past a rotating thin elliptic cylinder is studied for a medium at rest at infinity and for a parallel stream. The cylinder is considered infinitely long so that the problem is two-dimensional in space. For convenience in performing numerical analysis an elliptic co-ordinate system (η, θ) is introduced which is related to the Cartesian co-ordinates (x, y) through

$$x + iy = a \cosh(\eta + i\theta), \quad a > 0, \tag{1}$$

where a is the focal distance.

For an elliptic cylinder rotating with constant angular velocity $-\Omega$ (an assumption which is made throughout this paper) there is a steady-state solution for potential flow if the reference frame is fixed to the body (Lamb 1945, p. 88):

$$\psi'_R = -\tfrac{1}{4}\Omega a^2[\exp\{2(\eta_1 - \eta)\}(1 - 2\sin^2\theta) - 2(\cosh^2\eta - \sin^2\theta) + 2\cosh^2\eta_1 - 1], \tag{2}$$

so that

$$\psi'_R = 0 \quad \text{at} \quad \eta = \eta_1, \tag{3}$$

$$\psi'_R = \tfrac{1}{2}\Omega a^2(\cosh^2\eta - \sin^2\theta - \cosh^2\eta_1 + \tfrac{1}{2}) \quad \text{at} \quad \eta = \infty. \tag{4}$$

Here ψ'_R is the stream function, $\eta = \eta_1$ is the elliptic contour of the body and $+\Omega$ is now the angular velocity of the rotating fluid. An arbitrary constant in ψ'_R is chosen such that ψ'_R is zero on the body surface.

In the special case of a circular cylinder of radius r_1 with an imposed circulation the stream function is $\psi'_R = -\Omega r_1^2(\log r - \frac{1}{2}r^2/r_1^2)$ with $r^2 = x^2 + y^2$. Remarkably

this solution fulfils the no-slip boundary condition, and is thus a solution for viscous fluids. The torque necessary to maintain the steady motion is $T = 4\pi\mu\Omega r_1^2$, where μ is the dynamic viscosity. The case of transient viscous motion after an abrupt start was solved by Mallick (1957) and Lozupone (1967).

The more complicated problem of a rotating cylinder in a parallel stream with constant velocity U can be solved by superposition when linear theories are applied. The solution for steady-state viscous slow flow past a circular cylinder is given by Oseen (1927, p. 179), who superposed his solution for flow past a non-rotating cylinder on the solution for a rotating cylinder in quiescent fluid. The lift, drag and torque are

$$L = -\pi\rho r_1^2 U\Omega, \quad D = -\frac{4\pi\mu U}{\frac{1}{2} - \gamma - \log(\frac{1}{4}Ur_1/\nu)}, \quad T = 2\pi\mu\Omega r_1^2, \tag{5}$$

where γ is the Euler constant and ν the kinematic viscosity of the fluid. A solution through superposition also exists for potential flow. The solution for steady flow past a circular cylinder with circulation yields

$$L = -2\pi\rho r_1^2 U\Omega, \quad D = 0, \quad T = 0. \tag{6}$$

In the general case of the flow past a rotating elliptic cylinder the solution is unsteady. No slow-motion solution of the Oseen type is known to the authors. For potential flow superposition of (2) on the stream function ψ'_T for parallel flow past a fixed elliptic cylinder (Lamb 1945, p. 85) results in $\psi' = \psi'_R + \psi'_T$ with

$$\begin{aligned}\psi'_T = aU\,[&\sinh\eta\sin\theta\cos\Omega t' - \cosh\eta\cos\theta\sin\Omega t' \\ &- \exp(\eta_1 - \eta)\,(\sinh\eta_1\sin\theta\cos\Omega t' - \cosh\eta_1\cos\theta\sin\Omega t')].\end{aligned} \tag{7}$$

The lift (and the drag) is zero unless a circulation is superposed. The torque is $T = -\pi\rho a^2 U^2 \sin\Omega t'\cos\Omega t'$. Here t' denotes the time.

The potential-flow solution ψ' given by (2) and (7) contains one flow parameter in addition to the geometric parameter η_1. By making ψ' dimensionless according to $\psi' = aU\psi$ one obtains the Rossby number $Ro = U/\Omega a$ or, by using the chord $d = 2a\cosh\eta_1$, the parameter $Ro_{\frac{1}{2}d} = 2U/\Omega d$. Viscous fluid flow past a rotating cylinder in a fluid at rest is also characterized by one flow parameter only: the Reynolds number $R\tilde{e} = 4\Omega a^2/\nu$ or $R\tilde{e}_d = \Omega d^2/\nu$. However, the solutions for viscous fluid flow past a rotating cylinder in a parallel stream contain two flow parameters: the Rossby number $Ro_{\frac{1}{2}d}$ and the Reynolds number (defined either by $Re_d = Ud/\nu$ or $R\tilde{e}_d = \Omega d^2/\nu$).

A number of papers have been published in which flows with various combinations of $Ro_{\frac{1}{2}d}$ and Re_d (or $R\tilde{e}_d$) are discussed. These studies are based either on perturbation techniques or on numerical (finite-difference or finite-element) methods.

Moore (1957) investigated steady flow past a rotating circular cylinder for $Ro_{\frac{1}{2}d} \ll 1$ and $R\tilde{e}_d \gg 1$, where $Ro_{\frac{1}{2}d}$ is used as a perturbation parameter. This case represents a rapidly rotating body with a circular boundary layer in an otherwise irrotational flow. It may be recalled that for a circular cylinder three types of

potential flow can be distinguished: flow with two stagnation points at the body when $Ro_{\frac{1}{2}d} > 0{\cdot}5$, flow with one stagnation point when $Ro_{\frac{1}{2}d} = 0{\cdot}5$ and flow with no stagnation point at the body when $Ro_{\frac{1}{2}d} < 0{\cdot}5$. Moore's solution for $Ro_{\frac{1}{2}d} \ll 1$ falls in the last category. To the approximation considered the drag is zero and the lift equal to that in (6), which is the Kutta–Joukowsky formula.

Hocking (1974) considered the flow past a thin elliptic cylinder with end plates in a rapidly rotating fluid. The three-dimensional nature of the problem gives rise to Coriolis effects through the Ekman layer. In two-dimensional flows the Coriolis force does not appear (see §3). In Hocking's model the flow is kept steady by assuming that the Rossby number based on the distance between the end plates is vanishingly small.

For moderate values of $Ro_{\frac{1}{2}d}$ and Re_d the time-dependent flow past a circular cylinder was studied by Thoman & Szewcyzk (1966) using a finite-difference scheme. For $Re_d = 200$ and $Ro_{\frac{1}{2}d} = 1$ the flow has two stagnation points at the body, whereas for $Ro_{\frac{1}{2}d} \leqslant 0{\cdot}5$ there is no stagnation point. Results for other values of Re_d show that the extent of the circular flow region near the cylinder decreases with increasing Re_d when $Ro_{\frac{1}{2}d} \leqslant 0{\cdot}5$.

Recently, a finite-element technique was applied by Argyris & Mareczek (1974) to the steady slow motion of a rotating circular cylinder in a parallel channel.

This paper presents solutions for the general unsteady flow around rotating elliptic cylinders either in a fluid at rest or in a parallel stream. The non-rotating case was studied by Lugt & Haussling (1974) for $Re_d \leqslant 200$. Preliminary results from the rotating case and a description of the numerical methods involved were published in Lugt & Ohring (1974*a*, *b*).

2. A note on the reference frame

Steady motions imply the Eulerian form of flow description and the selection of one specific reference frame, i.e. the reference frame in which the flow becomes steady. In this steady-state system streamlines, pathlines and streaklines coincide. In unsteady flows no preferred reference frame exists, and the frame must be selected on the basis of other criteria. Furthermore, streamlines, pathlines and streaklines generally do not coincide.

For two-dimensional flow past a cylinder with constant translational speed $-U$ and angular velocity $-\Omega$, four different reference frames may be distinguished. If U^* and Ω^* are the translational and angular velocities of the body relative to the reference frame, these four different frames are as follows.

(1) $U^* = 0$, $\Omega^* \neq 0$; this frame is fixed to the body with regard to translation, but the body rotates relative to it.

(2) $U^* \neq 0$, $\Omega^* \neq 0$; the body is in translational and rotational motion relative to this frame. For $U^* = -U$ and $\Omega^* = -\Omega$ this frame is fixed to the fluid (at rest) at infinity.

(3) $U^* = 0$, $\Omega^* = 0$; this frame is fixed to the body.

(4) $U^* \neq 0$, $\Omega^* = 0$; this frame does not rotate relative to the body, but the body has a translational motion relative to it.

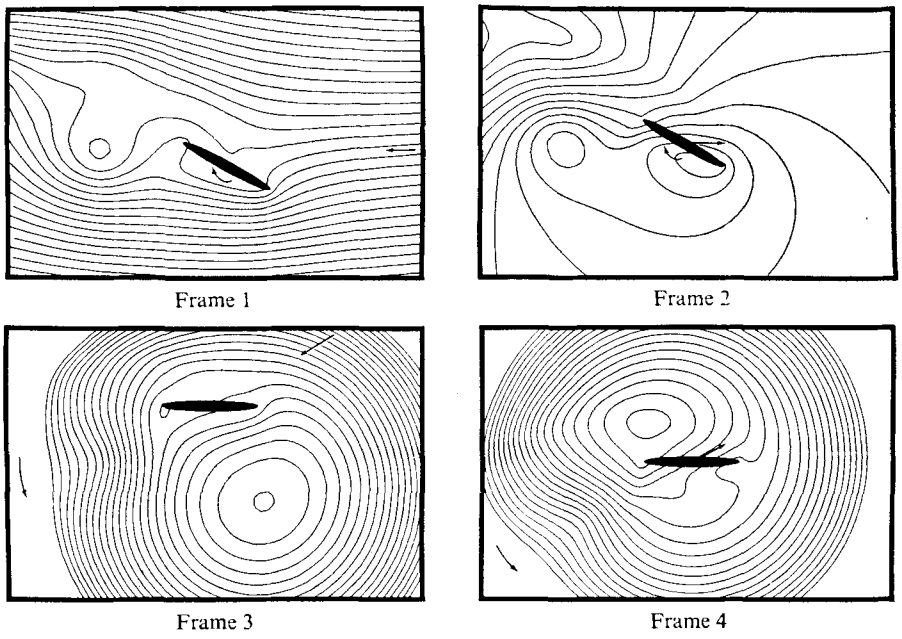

FIGURE 1. Streamline patterns for flow past a rotating elliptic cylinder in four different reference frames. $Re = 200$, $Ro = 2$, $\eta_1 = 0{\cdot}1$, $t = 10{\cdot}46$.

The behaviour of streamlines for the four different cases is illustrated in figure 1. For non-vanishing U^* and Ω^* these quantities are chosen to be $U^* = -U$ and $\Omega^* = -\Omega$. Since the streamlines are not invariant with respect to Galilean transformations (and certainly not invariant with respect to rotational transformations), all streamline patterns differ from each other. In contrast, the vorticity field (see figure 15*b*) is invariant and differs under rotational transformations only by a constant. The superiority of the vorticity field over the streamline patterns for explaining flow characteristics will be demonstrated in §5. It may be pointed out that the ability to produce vorticity patterns is one of the advantages of 'computer experiments' over wind-tunnel experiments, where the measurement of vorticity is very difficult.

In the study of streamline patterns the use of frame 1 is appealing because of its analogy to instantaneous streamline photos of a rotating body in a wind tunnel. Frame 3 is advantageous since the body contour is a streamline, and flow behaviour near the body (like separation) can be examined. Frames 2 and 4 are of less interest in the present investigation.

In time-dependent flows the identification of vortices and separated regions at the body becomes difficult. Although frame 3 is best suited (compared with the other three frames) for the discussion of flow separation, since the body contour is a streamline, the flow is still time dependent, and the definition of separation in a steady-state flow, $\omega = 0$ and $\partial\omega/\partial\theta < 0$ at $\eta = \eta_1$, does not hold. Only a reference frame fixed with respect to a 'separation line' and moving along the surface would make the flow locally steady (Rott 1956). However, in an approximate way, frame 3 is still useful to study flow separation at the body.

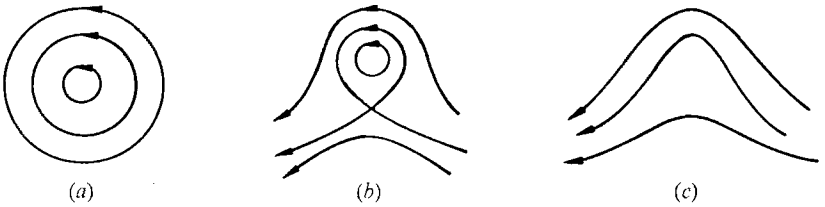

FIGURE 2. On a vortex (*a*) a constant parallel flow from right to left is superposed. In (*b*) the velocity of the parallel flow is small relative to the angular velocity of the vortex; in (*c*) the velocity of the parallel flow is large.

A difficulty similar to the problem of flow separation arises when the position of a vortex must be determined. Here again the definition of a vortex is not clear (Lugt 1974). Without elaborating on the difficulties two aspects are pointed out.

(i) A separated vortex (as distinct from flow separation) is defined to exist when a relative extremum of vorticity occurs in a homogeneous fluid. Such a vortex detached from the body manifests itself in streamline patterns consisting of either closed or wavy streamlines, depending on whether the vortex is at rest or moving relative to the reference frame (see figure 2). In figure 1 the separated vortex (which is about one plate length behind the body) is thus seen in frames 1 and 2 as closed streamlines and in frames 3 and 4 as wavy streamlines. Hence streamline pictures give information on the movement of vortices relative to the reference frame. The closed streamlines in frames 3 and 4 are due to the rotation of the frame and are circular at infinity. The centre of rotation coincides with the rotation centre of the body only when the translational motion vanishes.

(ii) The existence of the vorticity extremum may be used as the definition of a detached vortex. However, this definition does not hold for a vortex attached to a body, since the vorticity extremum occurs at the body surface. Either the recirculation region at the body surface is not considered a vortex, or the definition of a vortex must be based on circular or spiral pathlines in a local reference frame fixed to the centre of the vortex (Lugt 1974). The latter definition of an attached vortex is used in this paper.

3. Formulation of the problem

For the mathematical formulation of the physical problem outlined in § 1 the Navier–Stokes equations are used, expressed in terms of the vorticity ω' and the stream function ψ'. In η, θ co-ordinates the basic equations are

$$\frac{\partial \omega'}{\partial t'} + \frac{1}{a^2 h^2}\left[-\frac{\partial}{\partial \eta}\left(\frac{\partial \psi'}{\partial \theta}\omega'\right) + \frac{\partial}{\partial \theta}\left(\frac{\partial \psi'}{\partial \eta}\omega'\right)\right] = \nu \nabla'^2 \omega', \tag{8}$$

$$\nabla'^2 \psi' = \omega', \tag{9}$$

where $h^2 = \cosh^2 \eta - \cos^2 \theta$.

For the case of a rotating body in a fluid at rest at infinity the following dimensionless variables are introduced: $\omega' = \Omega\tilde{\omega}$, $\psi' = \Omega a^2\tilde{\psi}$, $t' = \tilde{t}/\Omega$, $R\tilde{e} = 4a^2\Omega/\nu$ and $\nabla' = a^{-1}\nabla$. Equations (8) and (9) then become

$$\frac{\partial\tilde{\omega}}{\partial\tilde{t}} + \frac{1}{h^2}\left[-\frac{\partial}{\partial\eta}\left(\frac{\partial\tilde{\psi}}{\partial\theta}\tilde{\omega}\right) + \frac{\partial}{\partial\theta}\left(\frac{\partial\tilde{\psi}}{\partial\eta}\tilde{\omega}\right)\right] = \frac{4}{R\tilde{e}}\nabla^2\tilde{\omega}, \tag{10}$$

$$\nabla^2\tilde{\psi} = \tilde{\omega}. \tag{11}$$

The boundary conditions for a frame fixed to the body are

$$\tilde{\psi} = 0, \quad \partial\tilde{\psi}/\partial\eta = 0 \quad \text{at} \quad \eta = \eta_1, \tag{12}$$

$$\partial\tilde{\psi}/\partial\theta = 0, \quad \partial\tilde{\psi}/\partial\eta = \cosh\eta\sinh\eta \quad \text{at} \quad \eta = \infty. \tag{13}$$

The velocity components $\tilde{v}_\eta$ and $\tilde{v}_\theta$ are related to $\tilde{\psi}$ by

$$\tilde{v}_\eta = -h^{-1}\partial\tilde{\psi}/\partial\theta, \quad \tilde{v}_\theta = h^{-1}\partial\tilde{\psi}/\partial\eta. \tag{14}$$

The computation of the case of a rotating body in a parallel flow requires a rescaling of (8) and (9). With $\omega' = (U/a)\omega$, $\psi' = Ua\psi$, $t' = (a/U)t$, $Ro = U/\Omega a$ and $Re = 2aU/\nu$ the basic equations become

$$\frac{\partial\omega}{\partial t} + \frac{1}{h^2}\left[-\frac{\partial}{\partial\eta}\left(\frac{\partial\psi}{\partial\theta}\omega\right) + \frac{\partial}{\partial\theta}\left(\frac{\partial\psi}{\partial\eta}\omega\right)\right] = \frac{2}{Re}\nabla^2\omega, \tag{15}$$

$$\nabla^2\psi = \omega. \tag{16}$$

The boundary conditions are (figure 3)

$$\psi = 0, \quad \partial\psi/\partial\eta = 0 \quad \text{at} \quad \eta = \eta_1, \tag{17}$$

$$\left.\begin{aligned} h^{-1}\partial\psi/\partial\theta &= \cos(\theta - t/Ro) \\ h^{-1}\partial\psi/\partial\eta &= \sin(\theta - t/Ro) + (hRo)^{-1}\cosh\eta\sinh\eta \end{aligned}\right\} \quad \text{at} \quad \eta = \infty, \tag{18}$$

with $\alpha(t) \equiv t/Ro$ being the angle of attack. It may be mentioned that the Coriolis term does not appear when the reference frame is changed from an inertial to a rotating frame. Thus the display of the four frames in figure 1 can be obtained by superposing a parallel flow and/or a rotating fluid, respectively.

The initial condition which simulates the abrupt start of the body from rest consists of the potential-flow solution, (2) and (7), and a vorticity sheet at the body surface enforcing the no-slip condition.

The drag, lift and moment coefficients are defined by

$$\left.\begin{aligned} C_D &= \text{drag}/\tfrac{1}{2}\rho U^2 a\cosh\eta_1, \\ C_L &= \text{lift}/\tfrac{1}{2}\rho U^2 a\cosh\eta_1, \\ C_M &= \text{torque}/\tfrac{1}{2}\rho U^2 a^2\cosh^2\eta_1. \end{aligned}\right\} \tag{19}$$

Each consists of two parts. The drag coefficient is the sum of drag due to pressure and drag due to friction: $C_D = C_{DP} + C_{DF}$ with

$$C_{DP} = \frac{4}{Re}\left[\tanh\eta_1\cos\alpha\int_0^{2\pi}\left(\frac{\partial\omega}{\partial\eta}\right)_1\sin\theta\,d\theta - \sin\alpha\int_0^{2\pi}\left(\frac{\partial\omega}{\partial\eta}\right)_1\cos\theta\,d\theta\right], \tag{20}$$

$$C_{DF} = \frac{4}{Re}\left[-\cos\alpha\int_0^{2\pi}\omega_1\sin\theta\,d\theta + \tanh\eta_1\sin\alpha\int_0^{2\pi}\omega_1\cos\theta\,d\theta\right]. \tag{21}$$

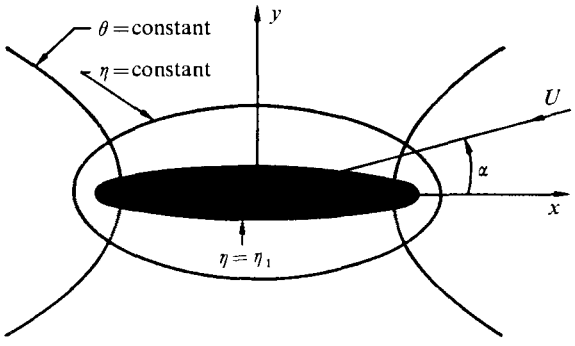

FIGURE 3. Elliptic co-ordinate system and definition of angle of attack.

The lift and moment coefficients may be expressed in a corresponding way (Lugt & Haussling 1974). For pure rotation ($U \equiv 0$) the torque is made dimensionless in the form

$$C_M = \text{torque}/\tfrac{1}{2}\rho\Omega^2 a^4 \cosh^4\eta_1, \tag{22}$$

with

$$C_{MP} = \frac{4}{R\tilde{e}\cosh^2\eta_1}\int_0^{2\pi}\left(\frac{\partial\tilde{\omega}}{\partial\eta}\right)_1 \sin^2\theta\, d\theta, \tag{23}$$

$$C_{MF} = \frac{8}{R\tilde{e}}\tanh\eta_1\int_0^{2\pi}\tilde{\omega}_1\, d\theta. \tag{24}$$

In this notation negative values of C_D, C_L and C_M mean respectively drag, lift in the direction of the Magnus force, and torque reinforcing the rotation of the body.

4. Numerical analysis

A computer program has been developed to construct solutions to the initial/boundary-value problem (15)–(18). Since a detailed description is given in Lugt & Ohring (1974*a*), it suffices to outline briefly the procedure, to explain the notation and to point out novel features of the program. The case of a rotating cylinder in a fluid at rest, which was not included previously and which is defined by (10)–(13), can be reduced to solving (15)–(18). All that is required is to set $Ro = 1$ and $Re = 0{\cdot}5R\tilde{e}$ and to modify the boundary conditions at infinity. For this case the boundary conditions applied in the numerical computation are

$$\tilde{\omega} = 2, \quad \partial\tilde{\psi}/\partial\eta = \cosh\eta\sinh\eta \quad \text{at} \quad \eta = \eta_{97} < \infty. \tag{25}$$

For a rotating body in a parallel stream the boundary conditions are

$$\partial\psi/\partial\eta = h\sin(\theta-\alpha) + Ro^{-1}\cosh\eta\sinh\eta, \quad \omega = 2/Ro$$

$$\text{at} \quad \eta = \eta_{97} < \infty, \quad 0 \leqslant \theta-\alpha \leqslant \tfrac{1}{2}\pi, \quad \tfrac{3}{2}\pi \leqslant \theta-\alpha \leqslant 2\pi \quad \text{(upstream half)}, \tag{26a}$$

$$\left.\begin{aligned} &\frac{\partial\omega}{\partial t} + \frac{1}{U}(\mathbf{U}.\nabla)\,\omega = 0 \\ &\left[\frac{\partial\mathbf{v}}{\partial t} + \frac{1}{U}(\mathbf{U}.\nabla)\,\mathbf{v} - 2\frac{a}{U}(\boldsymbol{\Omega}\times\mathbf{v}) - \nabla\frac{1}{2Ro^2}(\cosh^2\eta - \sin^2\theta)\right]_\theta = 0 \end{aligned}\right\}$$

$$\text{at} \quad \eta = \eta_{97} < \infty, \quad \tfrac{1}{2}\pi < \theta-\alpha < \tfrac{3}{2}\pi \quad \text{(downstream half)}, \tag{26b}$$

where **v** is the velocity vector and **U** the velocity vector of the parallel flow at infinity. The boundary conditions for the calculation of the non-rotating case are discussed in Lugt & Haussling (1974). The subscript θ denotes the θ component of the bracketed expression. If $\theta-\alpha < 0$, 2π must be added repeatedly until $\theta-\alpha \geqslant 0$.

The grid has been chosen in such a way that the infinite domain of integration is replaced by a finite network of points $\eta_1 + (i-1)\,\Delta\eta$, $(j-\frac{1}{2})\,\Delta\theta$ with $i = 1, \ldots, 97$ and $j = 1, \ldots, 96$; $\Delta\eta = 0{\cdot}04$.

Although the reference frame fixed to the body is advantageous for obtaining accurate values of the vorticity at and near the body surface, the overall ψ field is not accurate owing to the large values of ψ near the outer boundary (Lugt & Ohring 1974*b*). This can be remedied without losing the advantages of a grid fixed to the body by the transformation

$$\psi = \psi^* + (2Ro)^{-1}(\cosh^2\eta - \sin^2\theta), \quad \omega = \omega^* + 2/Ro. \tag{27}$$

The use of a grid rotating relative to the mainstream introduces a numerical difficulty. The discontinuities in $\partial\psi^*/\partial\eta$ and ω^* at $\eta = \eta_{97}$, $\theta-\alpha = \frac{1}{2}\pi$ and $\frac{3}{2}\pi$, which grow with advancing time and which were irrelevant for the calculation for non-rotating bodies, performed previously (Lugt & Haussling 1974), generate a disturbance every time an outer-boundary grid point moves from the downstream to the upstream half of the outer boundary. (The influence of the change from the upstream to the downstream half is negligible.) These disturbances are felt immediately throughout the fluid and cause large errors in the surface vorticity. This numerical phenomenon is aggravated at about $\alpha = \frac{5}{2}\pi$ and soon after renders the solution meaningless (for $\alpha > 3\pi$). It may be mentioned that at that time the vorticity has not yet reached the outer boundary. This difficulty has been overcome by smoothing out the discontinuities. The transition was done linearly over the outer-boundary arcs $\frac{1}{2}\pi < \theta-\alpha \leqslant \frac{3}{4}\pi$ and $\frac{5}{4}\pi \leqslant \theta-\alpha < \frac{3}{2}\pi$. The continuation of the solution in this manner is marked in figure 16 by circles (and the uncorrected solution by dots). The computation can then be continued even when the vorticity crosses the outer boundary.

The numerical analysis was carried out largely with the DuFort–Frankel scheme for solving the vorticity equation (15) and with the Hockney technique for solving the Poisson equation (16). This selection was made after preliminary studies with other methods (Lugt & Ohring 1974*a*).

Accuracy has been checked for $\Omega \equiv 0$ by comparing results with those obtained by Collins & Dennis (1974) for a circular cylinder from a series-expansion method and with experimental data by Honji (Lugt & Haussling 1974), and by using various $\Delta\theta$ and $\Delta\eta$. For a rotating body in a fluid at rest, the transient solution for a circular cylinder has been compared with the analytic solution of Mallick (1957). See §5. It may be pointed out that for small t ($< 0{\cdot}01$) the grid is coarse near the cylinder compared with the thickness of the vorticity layer. This affects the accuracy of the force and moment coefficients, which require the calculation of the vorticity gradient. Accuracy is also diminished for a rapidly rotating cylinder with $Ro_{\frac{1}{2}d} = 0{\cdot}5$ and $Re_d = 200$.

Computations were carried out in double precision on an IBM 360-91 computer.

Streamlines are plotted for the values $-3{\cdot}0$, $-2{\cdot}8$, ..., 0, ..., $+2{\cdot}8$, $+3{\cdot}0$, equivorticity lines for $-11{\cdot}0$, $-9{\cdot}0$, ..., $+9{\cdot}0$, $+11{\cdot}0$.

The following cases have been computed:

(*a*) Rotating cylinder in a fluid at rest:

$$\eta_1 = 0{\cdot}1, \quad R\tilde{e}_d = 400, \quad \Delta\tilde{t} = 0{\cdot}00375,$$
$$\eta_1 = 0{\cdot}1, \quad R\tilde{e}_d = 2000, \quad \Delta\tilde{t} = 0{\cdot}006,$$
$$\eta_1 = 3, \quad R\tilde{e}_d = 400, \quad \Delta\tilde{t} = 0{\cdot}2.$$

(*b*) Rotating cylinder in a parallel flow:

$$\eta_1 = 0{\cdot}1, \quad \alpha_0 = \pi, \quad Re = 200, \quad Ro = 2, \quad \Delta t = 0{\cdot}0025,$$
$$\eta_1 = 0{\cdot}1, \quad \alpha_0 = \tfrac{1}{2}\pi, \quad Re = 200, \quad Ro = 2, \quad \Delta t = 0{\cdot}0025,$$
$$\eta_1 = 0{\cdot}1, \quad \alpha_0 = \tfrac{1}{2}\pi, \quad Re = 200, \quad Ro = 0{\cdot}5, \quad \Delta t = 0{\cdot}00125.$$

For $\eta_1 = 0{\cdot}1$ (which may be considered as a 'plate'), $Ro \approx Ro_{\frac{1}{2}d}$, $Re \approx Re_d$ and $R\tilde{e} \approx R\tilde{e}_d$. Immediately after the abrupt start the time increment Δt is smaller than the above values, which are selected before numerical instability occurs.

5. Results

Rotating cylinders in a fluid at rest

Little is known about the behaviour of rotating elliptic cylinders at low Reynolds numbers. From the few solutions such as those for transient and steady motion of a rotating circular cylinder (Mallick 1957; Lozupone 1967) and from the purely translational motion of elliptic cylinders (Lugt & Haussling 1974), one infers that three different cases of the transient phase can be distinguished depending on the values of the parameters α, η_1 and $R\tilde{e}$. In the first case the approach to steady-state solutions is monotonic, for instance, in the transient motion of a rotating circular cylinder (figure 4) and in the translational motion of an elliptic cylinder with $\eta_1 = 0{\cdot}1$ and $Re_d = 15$. In the second case the approach to a steady state is oscillatory, for instance in the translational motion of a cylinder with $\alpha = 45°$, $\eta_1 = 0{\cdot}1$ and $Re_d = 30$. In the third case, a steady-state solution does not exist, and the transient, oscillatory period approaches an oscillatory (periodic) final state. An example is the translational motion of a cylinder with η_1 arbitrary and $Re_d > 45$, which represents a Kármán vortex street.

Numerical results for a rotating thin elliptic cylinder have been obtained for $\eta_1 = 0{\cdot}1$, $R\tilde{e} = 400 \approx R\tilde{e}_d$ and 2000. The C_M curves in figures 5 and 6 display oscillations which damp out to the steady-state value $C_M \approx 0{\cdot}25$ for $R\tilde{e} = 400$, whereas a periodic state is approached for $R\tilde{e} = 2000$. In this case the average value of C_M is 0·13 when $\tilde{t} \to \infty$. The steady-state value for a rotating circular cylinder is $C_M = 32\pi/R\tilde{e}_d$; that is, for $R\tilde{e}_d = 400$, $C_M = 0{\cdot}25$, and for $R\tilde{e}_d = 2000$, $C_M = 0{\cdot}05$. This means that for the lower Reynolds number the change in η_1 does not greatly affect the moment coefficient. For the higher Reynolds number, however, the torque decreases with larger η_1.

The oscillatory behaviour of the fluid motion can be explained using figures 7–12. After the abrupt start of the cylinder a vortex is shed from each edge and is

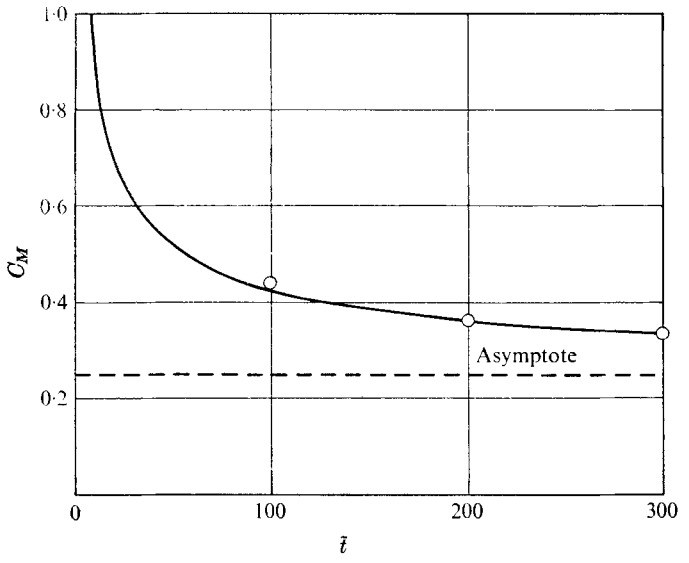

FIGURE 4. C_M vs. $\tilde{t}$ for an abruptly started rotating circular cylinder with $R\tilde{e}_d = 400$, $\eta_1 = 3$. ○, analytical values from Mallick (1957).

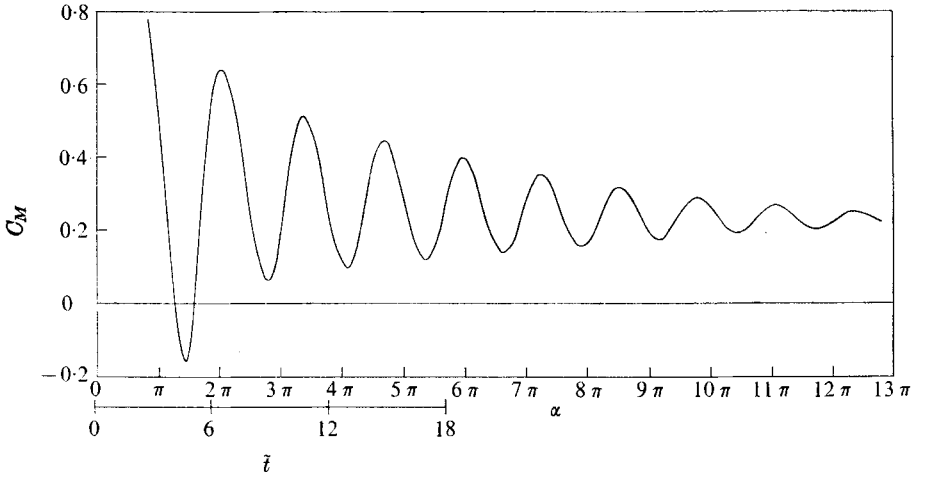

FIGURE 5. C_M *vs.* $\tilde{t}$ and α for an abruptly started rotating thin elliptic cylinder with $R\tilde{e} = 400$, $\eta_1 = 0{\cdot}1$.

clearly visible in the vorticity patterns. This vortex is swept towards the advancing opposite edge, where it causes a suction effect. This results in a minimum of C_M at $\tilde{t} = 4{\cdot}5$ for $R\tilde{e} = 400$. After the vorticity of this vortex has passed the advancing edge and amalgamated with the vorticity produced behind that edge, a relative maximum of C_M is reached at $\tilde{t} = 6{\cdot}45$. A new cycle starts in which a vortex of smaller strength than the earlier one is produced. This vortex follows the same path and is absorbed by the vortex behind the advancing edge. The effect of the vortex on C_M can be studied by plotting the integrand in (22) against θ (figure 10). From $\tilde{t} = 29$ on, a separated vortex cannot be detected in the computer

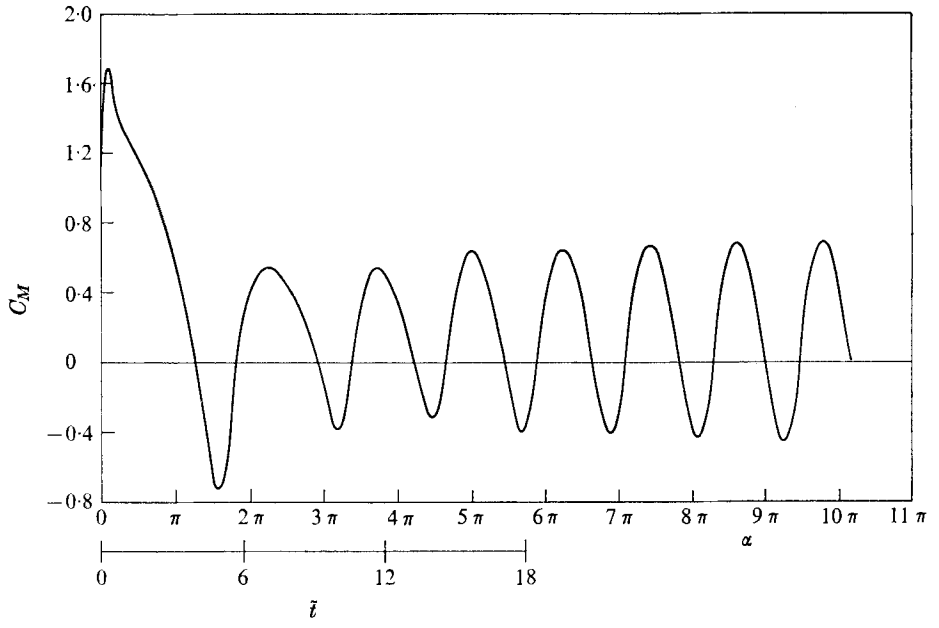

FIGURE 6. C_M *vs.* $\tilde{t}$ and α for an abruptly started rotating thin elliptic cylinder with $R\tilde{e} = 2000$, $\eta_1 = 0{\cdot}1$.

output, only a tongue of vorticity. Figure 9 shows the situation for $\tilde{t} = 40$, which is close to the steady state. The case $R\tilde{e} = 2000$ (figures 11 and 12) is similar to the case $R\tilde{e} = 400$ except that no damping is observed.

For a better understanding of the streamline patterns the potential-flow solution, which serves as the initial condition, is presented in figure 13. In a reference frame fixed to the body, two recirculatory regions occur at the surface of the cylinder. Shortly after the abrupt start of the body a Kutta-type flow past the edges develops, similar to the translational case discussed in Lugt & Haussling (1974). The detached vortices behind the edges, which are clearly visible in the vorticity patterns in figure 8, show up first at $\tilde{t} = 2{\cdot}10$ in the streamlines (figure 7). At $\tilde{t} = 1{\cdot}06$ the motion near the body is so slow that no streamlines are printed. From $\tilde{t} = 2{\cdot}10$ on attached vortices behind the edges due to viscous effects develop. By $\tilde{t} = 5{\cdot}19$ these attached vortices together with the detached vortices shed previously form four separated flow regions. At this time C_M reaches its relative minimum. At about $\tilde{t} = 6{\cdot}31$, when only two recirculatory regions at their largest extent exist, C_M reaches its relative maximum. For $R\tilde{e} = 2000$ the situation is similar although more clearly visible in the streamline patterns since the vortices are stronger than those for $R\tilde{e} = 400$.

Rotating cylinders in a parallel flow

The more complicated case of a rotating elliptic cylinder in a parallel stream requires the prescription of the two flow parameters Re and Ro in addition to the geometric parameters η_1 and α_0. $Re \approx Re_d$ is kept at 200 with $\eta_1 = 0{\cdot}1$. For $Ro \approx Ro_{\frac{1}{2}d}$ the values 2 and 0·5 are chosen.

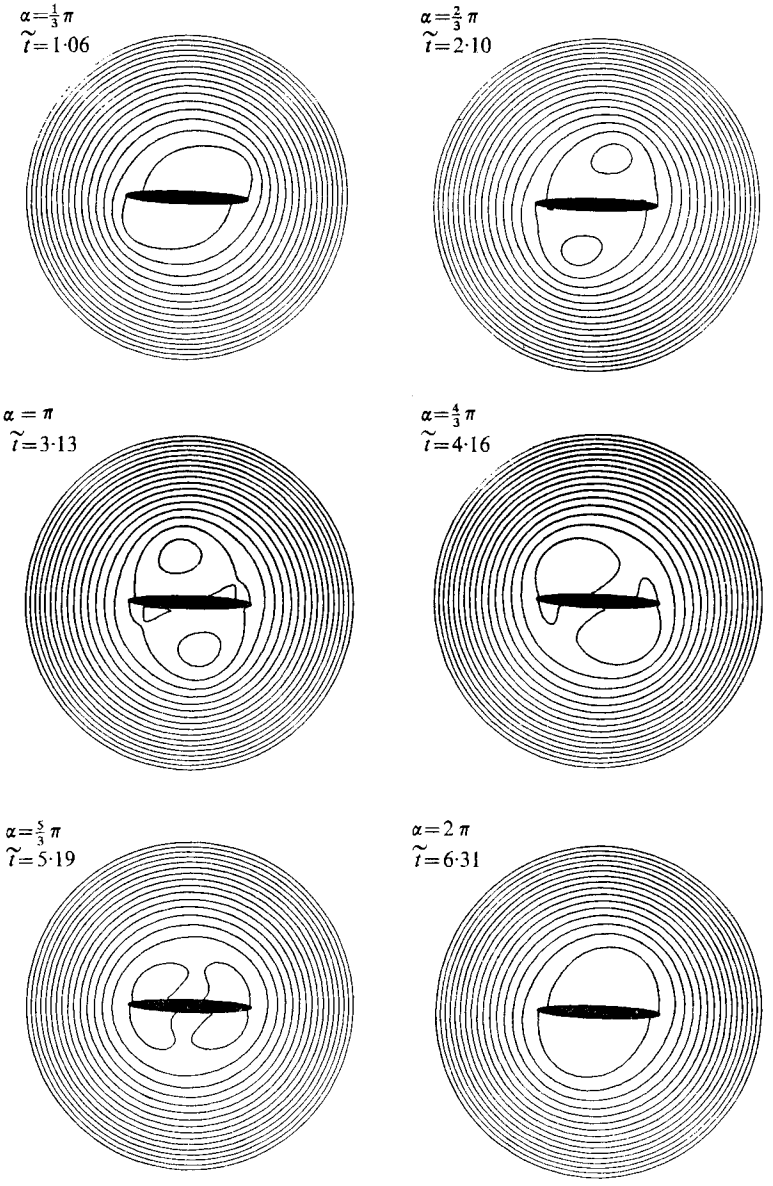

FIGURE 7. Sequence of streamlines around a rotating elliptic cylinder in a fluid at rest at infinity for $R\tilde{e} = 400$, $\eta_1 = 0{\cdot}1$, first revolution. The reference frame is fixed to the body, the fluid rotates anticlockwise. $\tilde{t}$ is given exactly (for three digits), α is given approximately.

In potential flows two types of motion may be considered. For $Ro = 0$ two recirculatory regions exist (figure 13). In the other limit, $Ro = \infty$, no such recirculatory regions occur. The numerical results show that at $Ro = 2$ (figure 14) there are still no recirculatory regions; however, when $Ro = 0{\cdot}5$ they do occur. It may be pointed out, as was done in the discussion of frame 3 in figure 1, that the closed streamlines are due to the rotation of the fluid, and that for $Ro > 0$ the rotation centre does not coincide with the centre of the rotating ellipse.

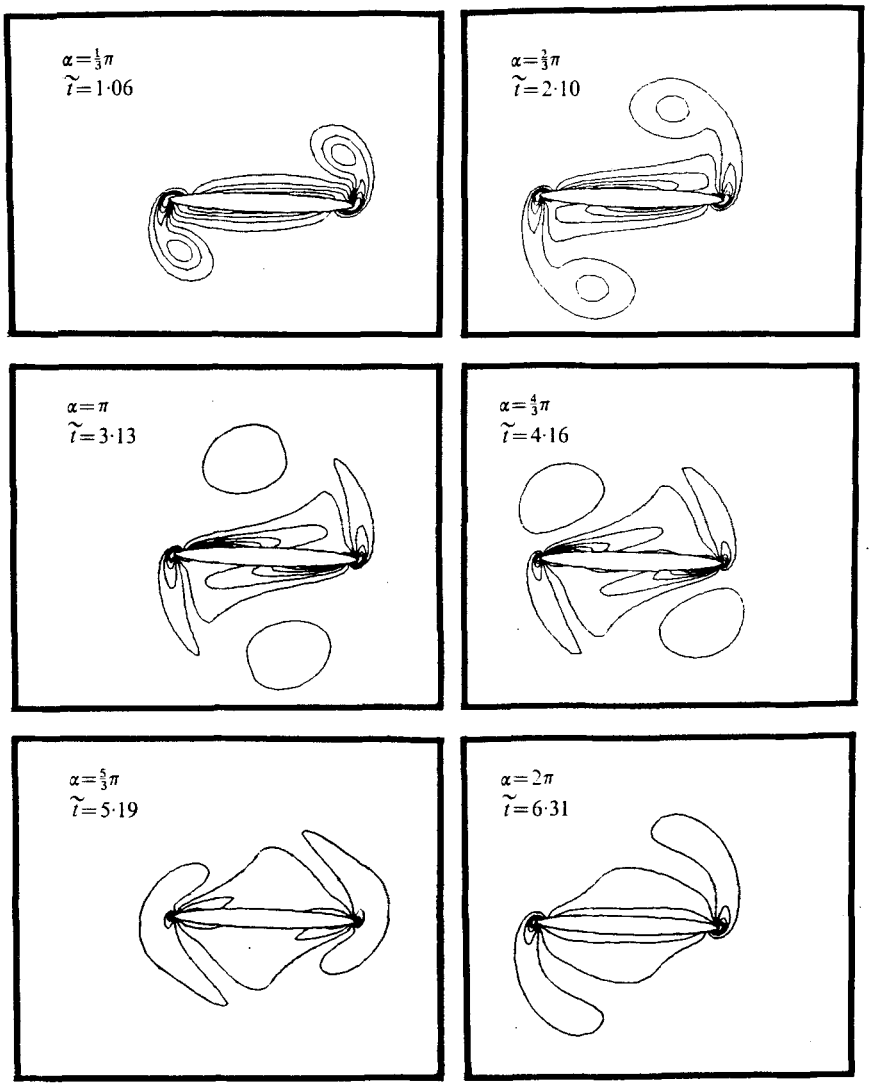

FIGURE 8. Sequence of equi-vorticity lines for the situation of figure 7.

With the potential-flow solution given as the initial condition, the flow development is displayed in figure 15 for the first revolution for the case $Re = 200$, $Ro = 2$, $\alpha_0 = \frac{1}{2}\pi$ and $\eta_1 = 0{\cdot}1$ (the continuation to $\alpha = 3\pi$ is given in Lugt & Ohring 1974*b*). As for a non-rotating plate perpendicular to the flow, two vortices are generated behind the two edges. At first, the vortex behind the advancing edge is stronger than the one behind the retreating edge because the relative flow speed is larger at the advancing edge. With the passing of time, however, the situation reverses, i.e. the vortex behind the retreating edge becomes stronger than the one behind the advancing edge. This change is due to the development of the newly generated vortices over a longer rotation period and to the influence of the vortices shed previously on the new ones. The vortex behind the retreating

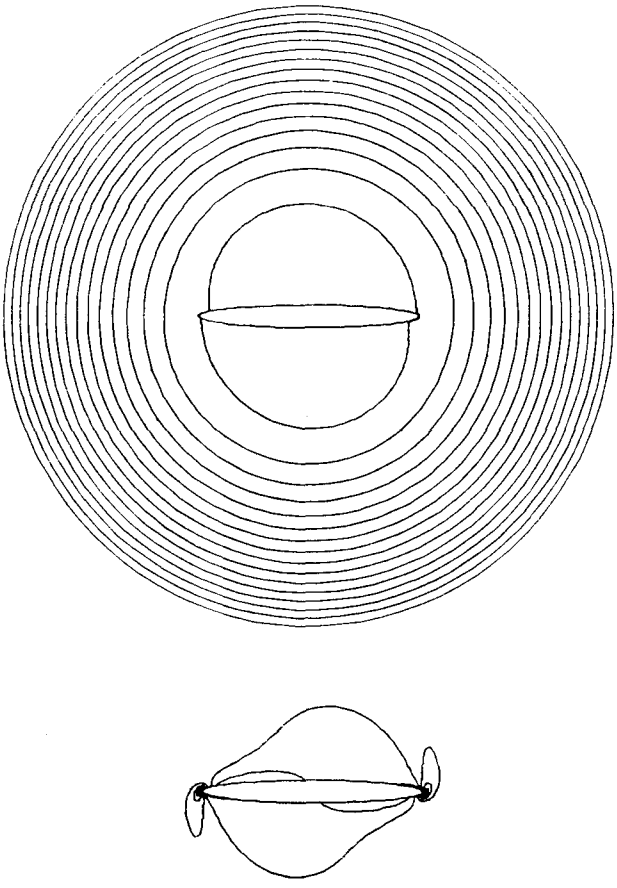

FIGURE 9. Streamlines and equi-vorticity lines for $R\tilde{e} = 400$, $\eta_1 = 0{\cdot}1$ in almost steady state ($\tilde{t} = 40$).

edge stays close to the body longer than did the previous one or the one behind the advancing edge. The latter vortex is stretched during the whole period $\pi + \frac{1}{3}\pi < \alpha < \pi + \frac{5}{6}\pi$. The streamlines clearly show the dominance of the vortex behind the advancing edge in the early phase ($1{\cdot}01 \leqslant t \leqslant 6{\cdot}26$) and the reverse afterwards. For the case $\alpha_0 = \pi$, which is presented in Lugt & Ohring (1974*a*), the initial situation of a stronger vortex behind the advancing edge does not occur. In all cases, however, a vortex is shed after every half-revolution $\Delta\alpha = \pi$.

More details of the flow behaviour can be obtained from the force and moment coefficients. Figure 16 shows these coefficients for $Re = 200$, $Ro = 2$ and $\alpha_0 = \frac{1}{2}\pi$ and π. These curves for $\alpha_0 = \frac{1}{2}\pi$ and π reveal a fast adjustment in the initial phase. From $\alpha = \frac{3}{2}\pi$ onwards the curves almost coincide. For part of the C_M curves the actual values are plotted using dots and circles so that the amount of scattering can be observed. The meaning of the circles was explained in §4.

The average values of the C_D and C_L curves are negative as expected since they represent the drag and the Magnus force on the body. The average lift-to-drag ratio is about unity. The C_M curve shows almost autorotating behaviour of the

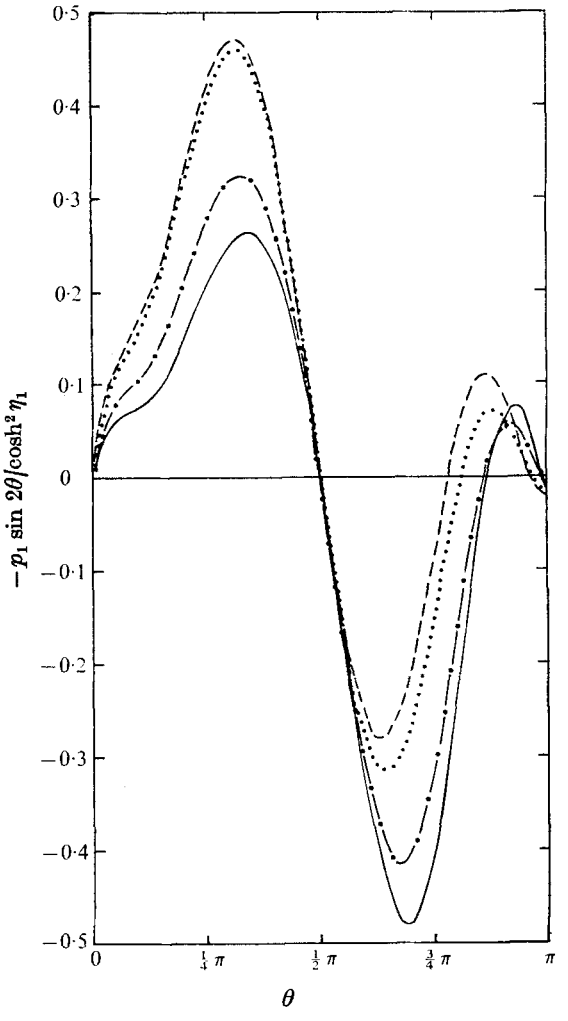

FIGURE 10. Local contribution to the torque *vs.* θ for $R\bar{e} = 400$, $\eta_1 = 0{\cdot}1$ and various times. $\theta = 0$ is at the right edge in figure 7 and increases anticlockwise. —, $\bar{t} = 4{\cdot}53$; – – –, $\bar{t} = 6{\cdot}41$; – · –, $\bar{t} = 8{\cdot}66$; · · · · ·, $\bar{t} = 10{\cdot}63$.

body. This means that the positive and negative values of C_M almost balance each other over one revolution, and that the kinetic energy of the parallel flow is almost sufficient for self-sustained spinning. Autorotation for such low Reynolds numbers is not surprising, since in wind-tunnel experiments autorotation has been observed for Reynolds numbers as low as 100 (Smith 1971).

The contribution of the frictional part of the total forces is small: C_{DF} and C_{LF} are an order of magnitude smaller than C_{DP} and C_{LP}. C_{MF} is so small, in general $C_{MF} < 0{\cdot}03$, that it can be neglected.

The analysis of C_D and C_L over one period of revolution reveals that the maximum drag ($-C_D$) occurs just before the plate is normal to the flow, and that the lift ($-C_L$) has its maximum value shortly after the plate reaches the horizontal

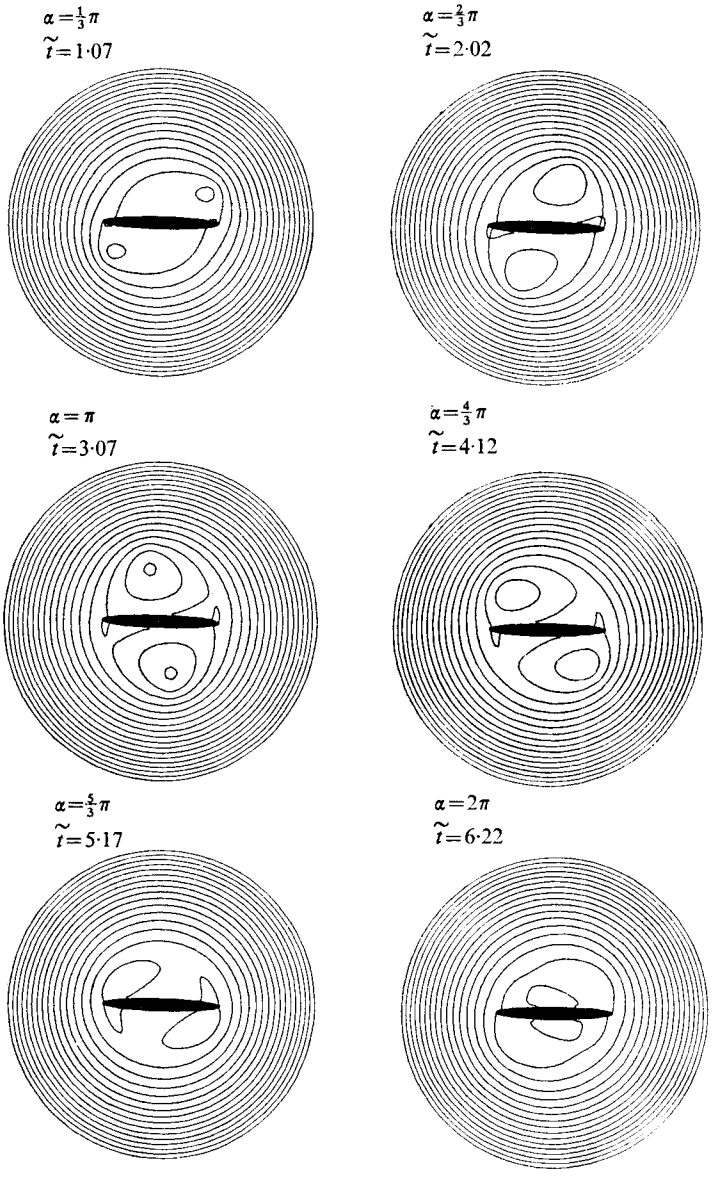

FIGURE 11. Sequence of streamlines around a rotating elliptic cylinder as in figure 7 but for $R\bar{e} = 2000$.

position. This roughly agrees with the behaviour of a non-rotating plate. The torque as a function of α behaves approximately like that of the corresponding potential flow, i.e. is proportional to $-\sin 2\alpha$. The deviations from this relation with respect to the phase and average value are due to the behaviour of the edge vortices.

The role of the edge vortices becomes clear when the results for $Ro = 2$ are compared with those for $Ro = 0{\cdot}5$ in figure 17. Although the behaviour of C_M

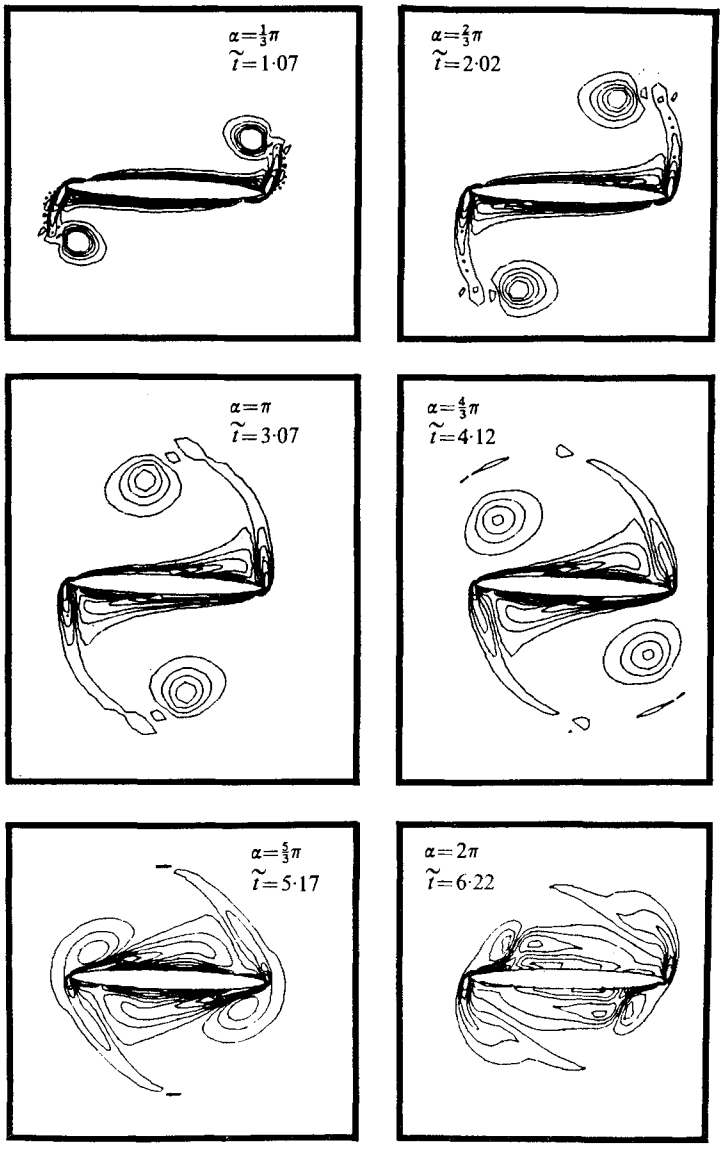

FIGURE 12. Sequence of equi-vorticity lines as in figure 8 but for $R\tilde{e} = 2000$.

with regard to α is similar, the two cases are essentially different. For $Ro = 0{\cdot}5$ the rotation is so strong relative to the translation that the vortex behind the retreating edge now develops on the other side of the plate. This means that the vortices generated at the edges always rotate in the direction opposite to the body rotation, as in the case of a rotating body in the fluid at rest (figure 8). Furthermore, the vortices are shed so slowly that they interfere with the opposite edges. This makes the process of vortex shedding much more complicated (figures 18 and 19).

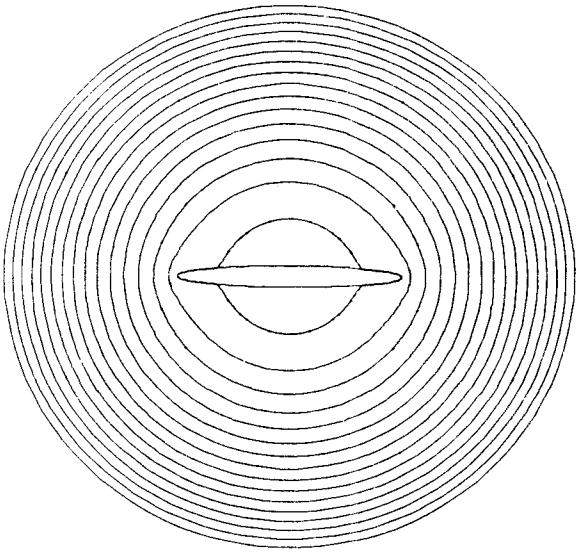

FIGURE 13. Potential flow around a rotating elliptic cylinder with $\eta_1 = 0{\cdot}1$. The reference frame is fixed to the body; the flow is steady.

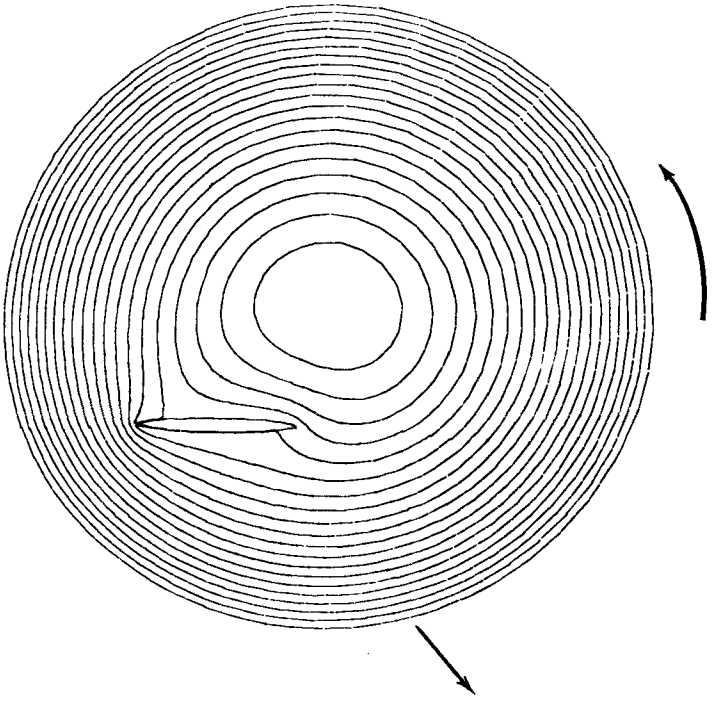

FIGURE 14. Potential flow around a rotating elliptic cylinder in a parallel flow with $Ro = 0{\cdot}5$, $\eta_1 = 0{\cdot}1$ and $\alpha = 135°$. The reference frame is fixed to the body; the flow is unsteady.

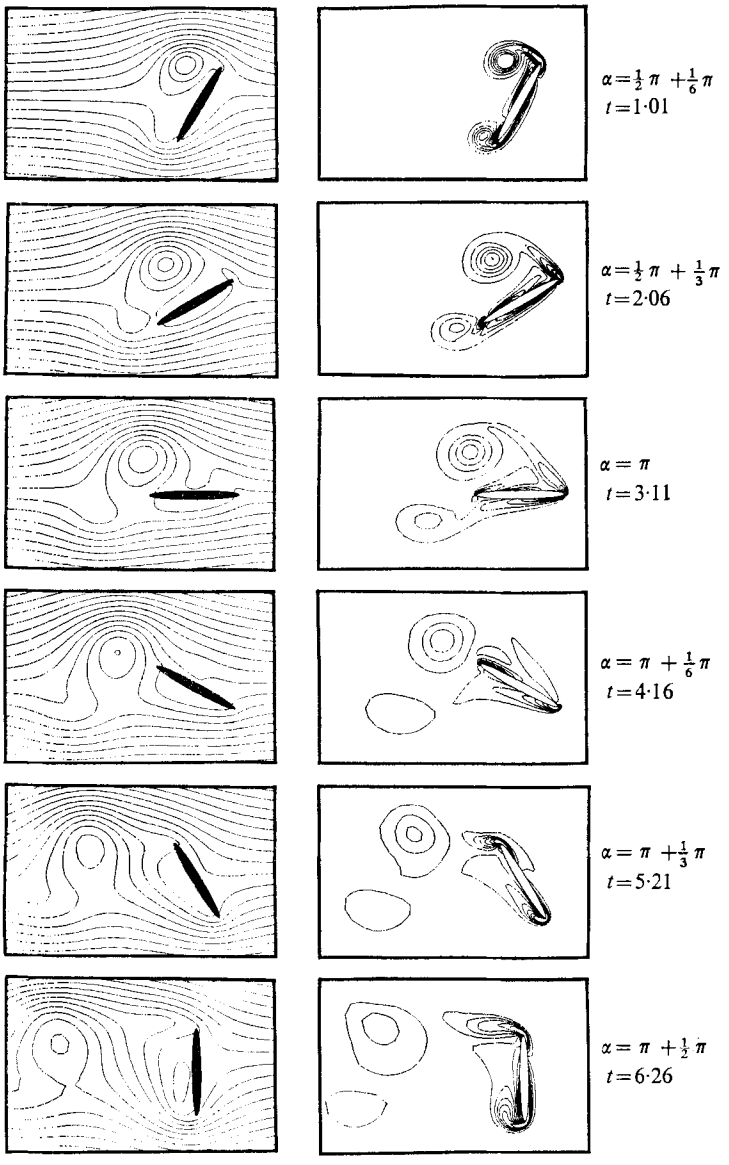

FIGURE 15(*a*). For caption see next page.

The average values of C_D and C_L in figure 17 are negative as in the previous case although the average C_D curve tends to become positive in time. This means that the drag would then become a thrust. The average C_M values are positive. Hence a torque must be applied to keep the body rotating. This behaviour differs from that for $Ro = 2$, for which autorotation is observed. The explanation must be sought in the difference in vortex generation behind the edges.

Immediately after the start a vortex develops behind the retreating edge in the form of a vorticity tongue (figure 18, $t = 0{\cdot}26$). After half a revolution this

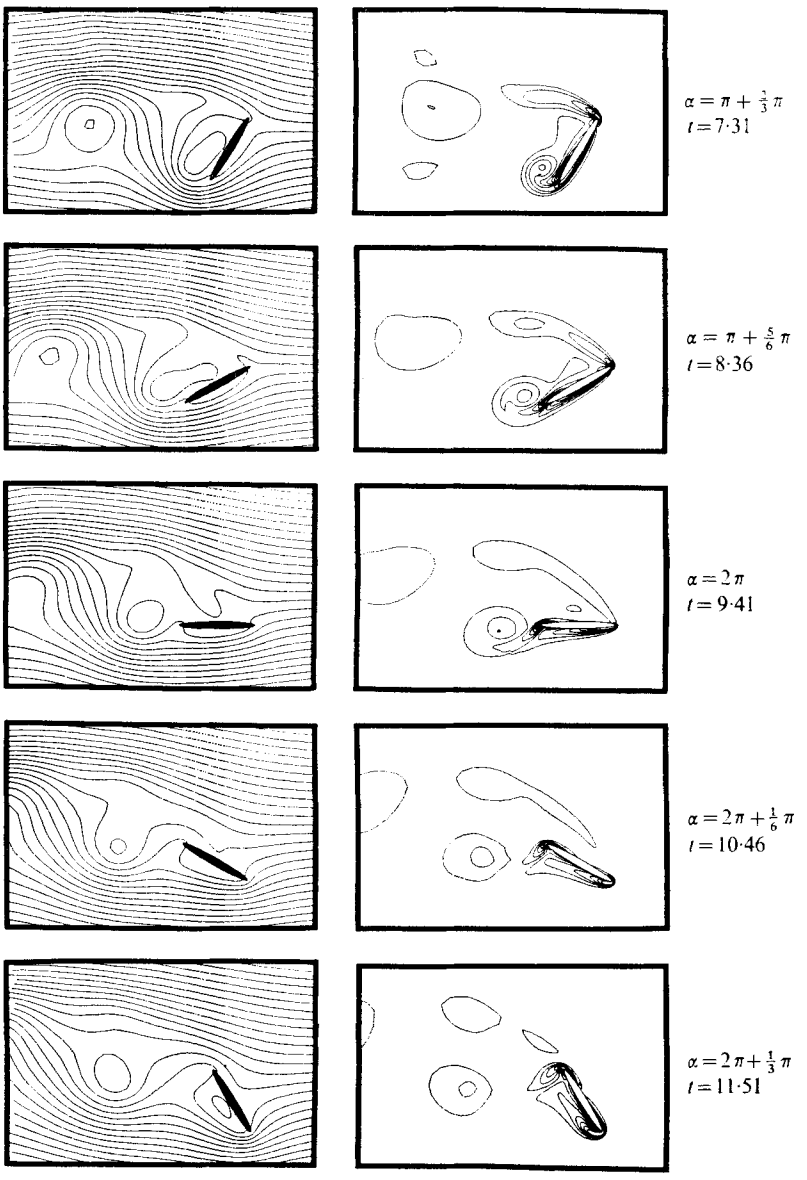

FIGURE 15. Sequence of streamlines and equi-vorticity lines around a rotating elliptic cylinder in a parallel flow for $Re = 200$, $Ro = 2$, $\eta_1 = 0{\cdot}1$, $\alpha_0 = \frac{1}{2}\pi$, first revolution. The streamlines are computed in frame 1.

vortex separates at about $t = 1{\cdot}822$ and moves away from the body ($t = 3{\cdot}135$). The advancing vortex is stronger from the beginning, separates before $t = 0{\cdot}51$ and moves away after the body has completed its first revolution ($t = 3{\cdot}135$). Thus, at this time the two vortices which were generated at the edges after the abrupt start are about half a plate length behind the body and ready to be

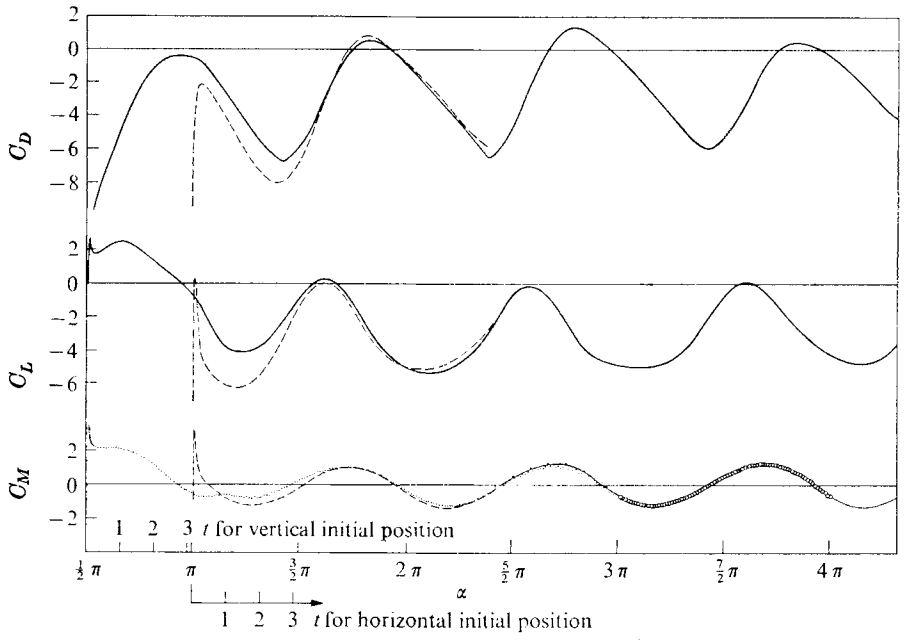

FIGURE 16. C_D, C_L, and C_M *vs.* α (or time) for $Re = 200$, $Ro = 2$, $\eta_1 = 0{\cdot}1$, $\alpha_0 = \frac{1}{2}\pi$ and π. —, ...ooo, vertical initial position; - - -, horizontal initial position.

swept away. Since both vortices are rotating anticlockwise it is expected that they will revolve anticlockwise about each other as they move away from the body.

Later, however, the process of vortex shedding becomes different as can be seen in the sequence of flow patterns for the fourth revolution in figure 19. The vortex at the retreating edge, which begins to develop at $t = 9{\cdot}95$, behaves similarly to that in the first revolution until about $t = 11{\cdot}26$. Comparing this instant with $t = 1{\cdot}822$ in figure 18, one observes that at $t = 11{\cdot}26$ the vortex is not left behind and does not move downstream but collides with the opposite, advancing edge and is pushed upstream. The vortex remains close to the plate for another cycle. This means that during the first four revolutions the period during which a vortex develops and is shed has increased from 2π to 3π. The transient state from the start to the quasi-steady state is thus not only much longer than for $Ro = 2$ but also shows a change in phase. (In fact, the periodic state has not been reached at the end of the computer run when $\alpha = 11\pi$; see figure 17.) Another difference between the first and the fourth revolution at $Ro = 0{\cdot}5$ occurs when the vortices are about to escape. Behind the retreating edge at the wake side of the body, clockwise vorticity is induced by the anticlockwise vortices ($t = 10{\cdot}48$ or $12{\cdot}04$), which results in the shedding of a clockwise vortex. In contrast to the situation at $t = 3{\cdot}135$, the vortex pair in the wake of the body at $t = 11{\cdot}01$ or $12{\cdot}57$ shows opposite rotation. Its path is directed towards the upper left corner in figure 19. The counter-rotation of the strong lower vortex of the pair supports this upward movement of the streamlines due to the rotating body (figure 20). A comparison

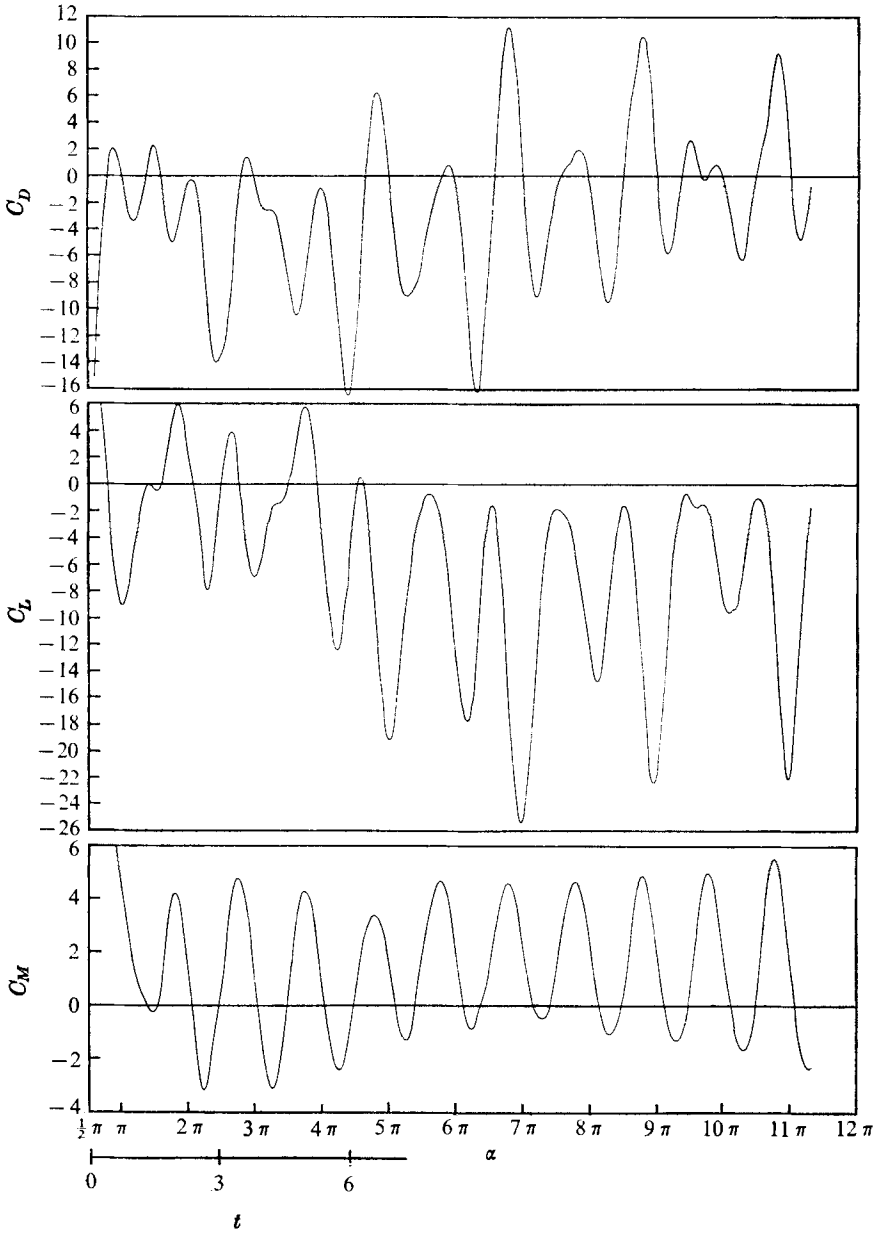

FIGURE 17. C_D, C_L and C_M *vs.* α (or time) for $Re = 200$, $Ro = 0{\cdot}5$, $\eta_1 = 0{\cdot}1$ and $\alpha_0 = \frac{1}{2}\pi$.

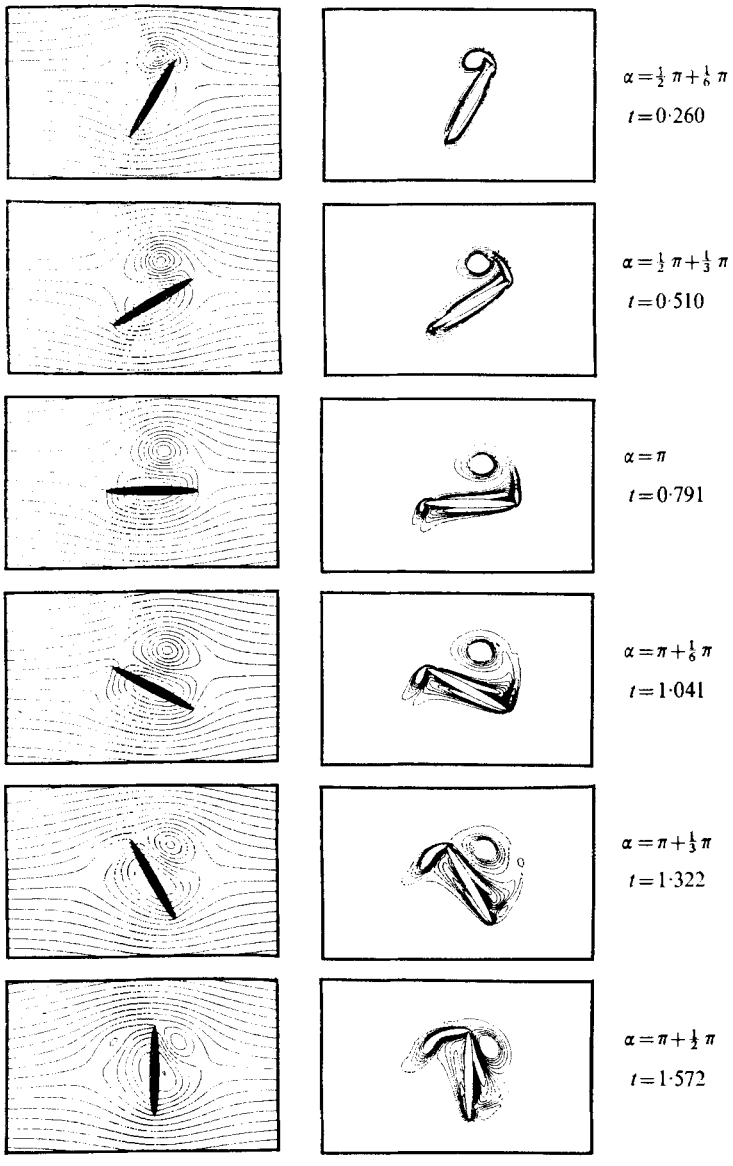

FIGURE 18(*a*). For caption see next page.

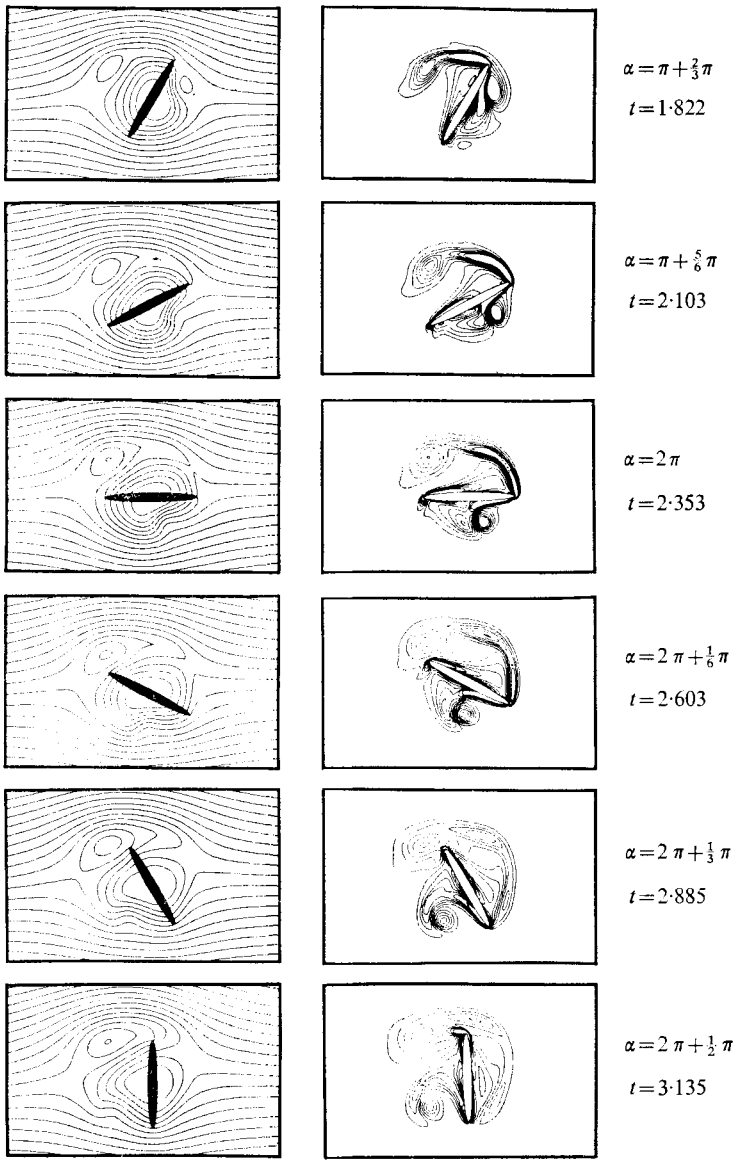

(*b*)

FIGURE 18. Sequence of streamlines and equi-vorticity lines for $Re = 200$, $Ro = 0{\cdot}5$, $\eta_1 = 0{\cdot}1$, $\alpha_0 = \frac{1}{2}\pi$, first revolution. The streamlines are computed in frame 1.

of the two half-cycles $6\pi+\frac{1}{2}\pi < \alpha \leqslant 7\pi+\frac{1}{2}\pi$ and $7\pi+\frac{1}{2}\pi < \alpha \leqslant 8\pi+\frac{1}{2}\pi$ shows that they do not completely match (figures 19 and 20). This can probably be explained by the phase change of the vortex shedding.

It is also conjectured that the drastic change in amplitude of C_D and C_L in figure 17 after every half-revolution π is due to that phase adjustment. A rigorous proof for this is difficult with the numerical data available. The deviations of the

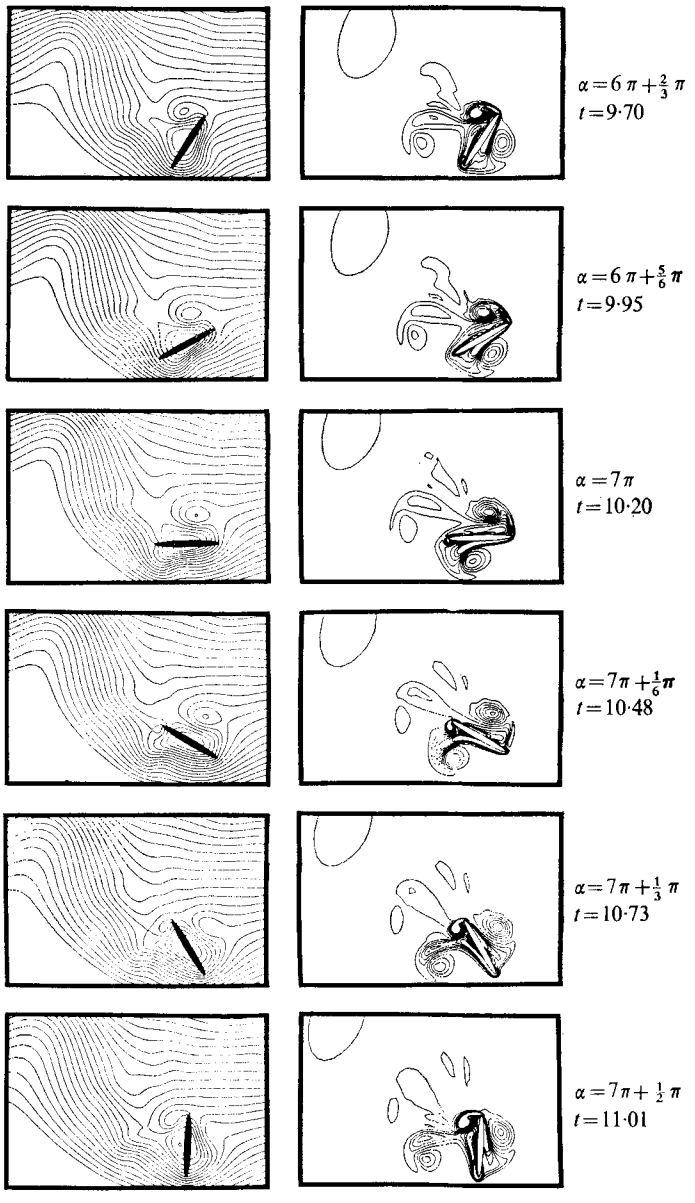

FIGURE 19(*a*). For caption see next page.

flow characteristics immediately at the body from one half-revolution to the other are quite subtle, although the resulting differences in C_D and C_L are large.

No great change in the amplitudes of the C_M curve in figure 17 is apparent. This means that the distance between the geometric centre of the body and the centre of pressure varies in such a way that it compensates for the variation in the C_D and C_L amplitudes.

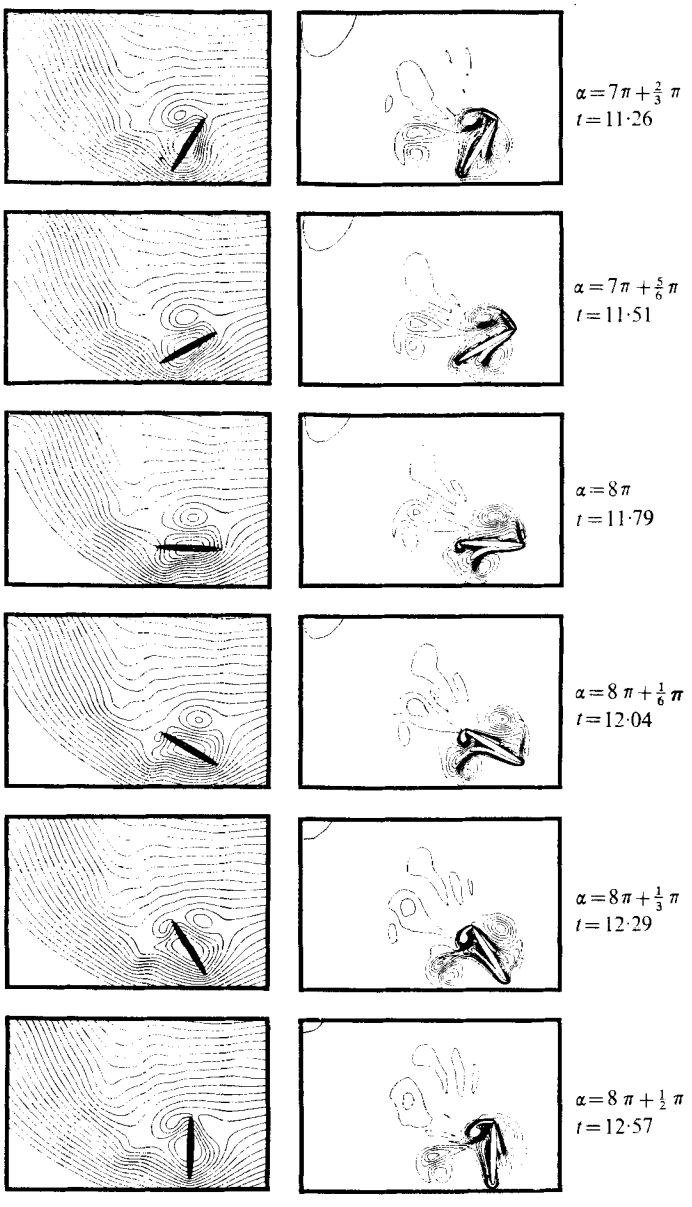

(*b*)

FIGURE 19. Sequence of streamlines and equi-vorticity lines for $Re = 200$, $Ro = 0{\cdot}5$, $\eta_1 = 0{\cdot}1$, $\alpha_0 = \frac{1}{2}\pi$, fourth revolution. The streamlines are computed in frame 1.

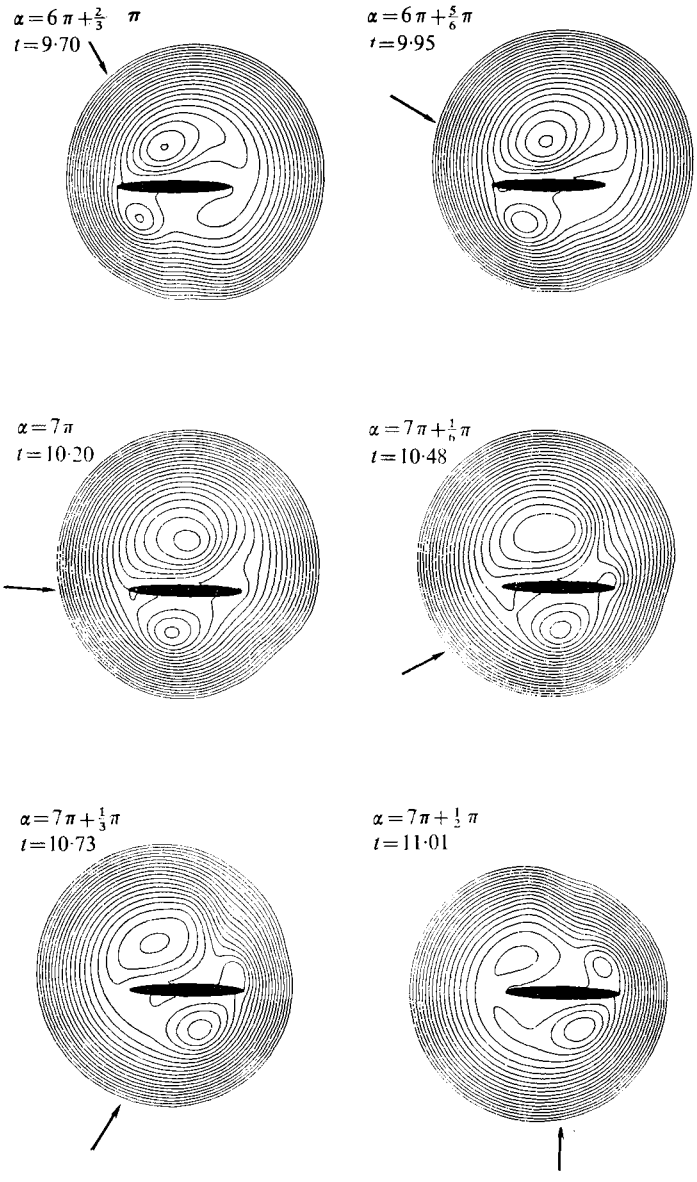

FIGURE 20(*a*). For caption see next page.

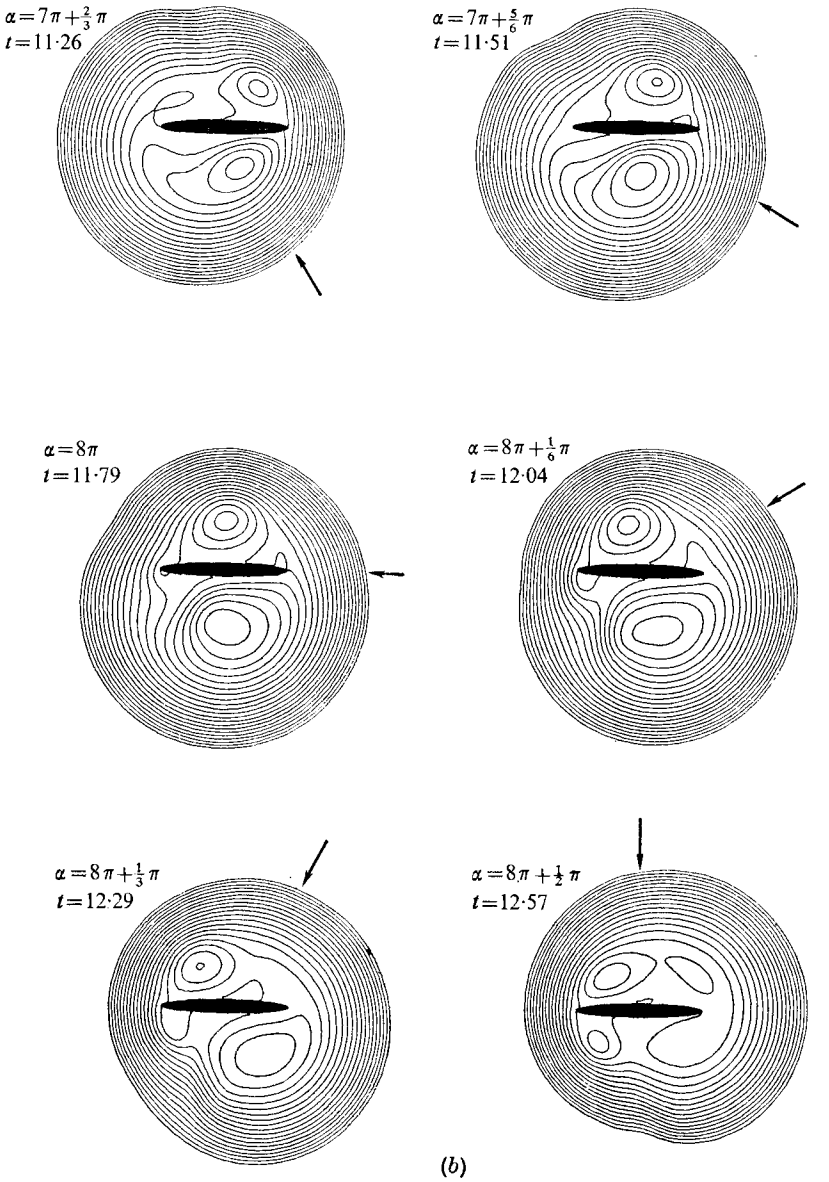

(*b*)

FIGURE 20. Same situation as in figure 19 but in frame 3.

The difference in the average value of C_M between $Ro = 2$ and $0{\cdot}5$ is explained by the strength of the vortex behind the retreating edge. The thin boundary layer from the front stagnation point to the retreating edge (figure 15, $t = 8{\cdot}36$) causes a torque which supports the body's rotation. The comparatively long time available for the development of this layer results in the production and shedding of a relatively large amount of clockwise vorticity. In contrast to this, such a boundary layer in front of the body cannot develop for $Ro = 0{\cdot}5$ because of the presence of the front vortex ($t = 9{\cdot}95$ in figures 19 and 20). The influence of the various vortices on the local moment coefficient is demonstrated in figure 21. For

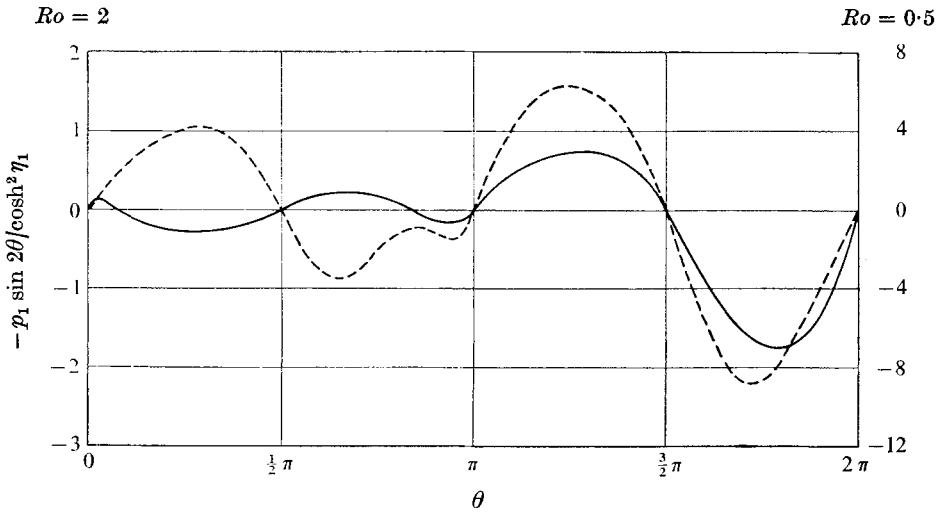

FIGURE 21. Local contribution to the torque *vs.* θ for $Re = 200$, $\eta_1 = 0{\cdot}1$. —, $Ro = 2$ at $t = 10{\cdot}46$; - - -, $Ro = 0{\cdot}5$ at $12{\cdot}04$. In figures 15 and 19, $\theta = 0$ is for these instants at the retreating edge and increases anticlockwise.

$Ro = 0{\cdot}5$ two phenomena counteract the tendency of the retreating-edge flow to support the body rotation: (i) the presence of the front vortex, causing a suction effect ($0 < \theta < \frac{1}{2}\pi$), and (ii) the opposing influence of the strong vortex behind the advancing edge ($\pi < \theta < \frac{3}{2}\pi$), which is large relative to the supporting part ($\frac{3}{2}\pi < \theta < 2\pi$).

The authors would like to thank Dr H. J. Haussling for helpful discussions, in particular for suggesting the transformation (27).

REFERENCES

ARGYRIS, J. H. & MAREČZEK, G. 1974 Finite-element analysis of slow incompressible viscous fluid motion. *Ing. Arch.* **43**, 92.

COLLINS, W. M. & DENNIS, S. C. R. 1974 Symmetrical flow past a uniformly accelerated circular cylinder. *J. Fluid Mech.* **65**, 461.

HOCKING, L. M. 1974 The flow past a cylinder in a rotating frame. *Z. angew. Math. Phys.* **25**, 486.

LAMB, H. 1945 *Hydrodynamics*, 6th edn. Dover.

LOZUPONE, V. 1967 Diffusione della vorticitá in un fluido internamente delimitato da un cilindro in rotazione impulsiva. *Ricerca Scientifica*, **37**, 1218.

LUGT, H. J. 1974 The dilemma of defining a vortex. *Naval Ship R. & D. Center, Tech. Note*, CMD-11-74.

LUGT, H. J. & HAUSSLING, H. J. 1974 Laminar flow past an abruptly accelerated elliptic cylinder at 45° incidence. *J. Fluid Mech.* **65**, 711.

LUGT, H. J. & OHRING, S. 1974*a* Efficiency of numerical methods in solving the time-dependent two-dimensional Navier–Stokes equations. *Proc. Int. Conf. Numerical Methods in Fluid Dyn., Southampton*, p. 65. New York: Crane, Russak & Co.

LUGT, H. J. & OHRING, S. 1974*b* Rotating thin elliptic cylinder in a parallel viscous fluid flow. *Proc.* 4th *Int. Conf. Numerical Methods in Fluid Dyn., Boulder. Lecture Notes in Phys.* vol. 35, p. 257. Springer.

MALLICK, D. D. 1957 Nonuniform rotation of an infinite circular cylinder in an infinite viscous liquid. *Z. angew. Math. Mech.* **37**, 385.

MOORE, D. W. 1957 The flow past a rapidly rotating circular cylinder in a uniform stream. *J. Fluid Mech.* **2**, 541.

OSEEN, C. W. 1927 *Hydrodynamik*, p. 179. Leipzig: Akademische Verlagsgesellschaft.

ROTT, N. 1956 Unsteady viscous flow in the vicinity of a stagnation point. *Quart. Appl. Math.* **13**, 444.

SMITH, E. H. 1971 Autorotating wings: an experimental investigation. *J. Fluid Mech.* **50**, 513.

THOMAN, D. C. & SZEWCZYK, A. A. 1966 Numerical solutions of time dependent two dimensional flow of a viscous, incompressible fluid over stationary and rotating cylinders. *Univ. Notre Dame, Dept. Mech. Engng, Tech. Rep.* no. 66–14.